

Modal locking between vocal fold oscillations and vocal tract acoustics

Tiina Murtola^{1,2)}, Atte Aalto^{2,3)}, Jarmo Malinen²⁾, Daniel Aalto^{4,5)}, Martti Vainio⁴⁾

¹⁾Dept. of Signal Processing and Acoustics, Aalto University, Finland

²⁾Dept. of Mathematics and Systems Analysis, Aalto University, Finland

³⁾Luxembourg Centre for Systems Biomedicine, University of Luxembourg, Luxembourg

⁴⁾Institute of Behavioural Sciences (SigMe group), University of Helsinki, Finland

⁵⁾Communication Sciences and Disorders, University of Alberta, Canada.

1 Summary

During voiced speech, vocal folds interact with the vocal tract acoustics. The resulting glottal source–resonator coupling has been observed using mathematical and physical models as well as in *in vivo* phonation. We propose a computational time-domain model of the full speech apparatus that contains a feedback mechanism from the vocal tract acoustics to the vocal fold oscillations. It is based on numerical solution of ordinary and partial differential equations defined on vocal tract geometries that have been obtained by magnetic resonance imaging. The model is used to simulate rising and falling pitch glides of [a, i] in the fundamental frequency (f_o) interval [145 Hz, 315 Hz]. The interval contains the first vocal tract resonance f_{R1} and the first formant F_1 of [i] as well as the fractions of the first resonance $f_{R1}/5$, $f_{R1}/4$, and $f_{R1}/3$ of [a]. The glide simulations reveal a locking pattern in the f_o trajectory approximately at f_{R1} of [i]. The resonance fractions of [a] produce perturbations in the pressure signal at the lips but no locking.

1 Introduction

The classical source–filter theory of vowel production assumes that the source (i.e., the vocal fold vibration) operates independently of the filter (i.e., the vocal tract, henceforth VT) whose resonances modulate the resulting sound [1, 2]. Even though this approach captures a wide range of phenomena in speech production, some observations remain unexplained by the source–filter model lacking feedback. The purpose of this article is to address some of these observations using computational modelling.

In this work, simulations where the fundamental frequency (f_o) rises and falls over the range [145 Hz, 315 Hz] are considered for vowels [a] and [i]. Similar glides recorded from eleven female test subjects are treated in the companion article [3]. Such

glides are particularly interesting when the f_o range intersects an isolated acoustic resonance of the supra- or subglottal cavity. Since the lowest formant F_1 usually lies high above f_o in adult male phonation, this situation is more typical in females and children when they are producing vowels with low F_1 such as [i]. As reported in Section 5, simulations reveal (in addition to other observations) a characteristic locking behaviour of f_o at the VT acoustic resonance¹ $f_{R1} \approx F_1$.

This article has two equally important objectives. Firstly, we pursue better understanding of the time-domain dynamics of glottal pulse perturbations near f_{R1} of [i]. An acoustic and flow-mechanical model of the speech apparatus is a well-suited tool for this purpose. Secondly, we introduce and validate a computational model that meets these requirements. The proposed model has been originally designed to be a glottal source for a high-resolution 3D computational acoustics model of the VT which is being developed for medical purposes. There is also an emerging application for such models as a development platform of speech signal processing algorithms [5, 6, 7]. Since perturbations of f_o near F_1 are a widely researched, yet quite multifaceted phenomenon, as discussed next, it is a good candidate for model validation experiments.

The simulations carried out in this article indicate special kinds of perturbations in vocal folds vibrations near a VT resonance. The mere existence of such perturbations is not surprising considering the wide range of existing literature. Since the seminal work of [8], a wide range of glottal source perturbation patterns related to acoustic loading has been investigated. Experiments were carried out in [9] on excised larynges mounted on a resonator to determine how glottal amplitude ratio changes with the subglottal resonator length. Physical models were used in [10] with a subglottal resonator to study phonation onsets and offsets, and in [11] with sub- and supraglottal resonators to study phonation onsets. The latter also considered

¹The notation of [4] is used to differentiate resonances and formants though, of course, we expect $f_{Rj} \approx F_j$ for $j = 1, 2, \dots$

39
40
41
42
43
44
45
46
47
48
49
50
51
52
53
54
55
56
57
58
59
60
61
62
63
64
65
66
67
68
69
70
71
72
73
74
75
76
77
78

79 the dynamics of frequency jumps as the natural fre-
 80 quency of their physical model was varied over time.
 81 Similarly, a physical model of phonation with a tubular,
 82 variable length supraglottal resonator was studied
 83 in [12, 13], and it was used to validate a flow-acoustic
 84 model somewhat resembling the one proposed in this
 85 article.

86 The source-filter interaction problem was ap-
 87 proached in [14] using both reasoning based on
 88 sub- and supraglottal impedances and a non-
 89 computational flow model as well as computational
 90 model comprising a multi-mass vocal fold model and
 91 wave-reflection models of the subglottal and supra-
 92 glottal systems. A two-mass model of vocal folds,
 93 coupled with a variable-length resonator tube, was
 94 used in [15], and pitch glides were simulated using a
 95 four-mass model to analyse the interactions between
 96 vocal register transitions and VT resonances in [16].

97 These works reveal a consistent picture of the ex-
 98 istence of perturbations caused by resonant loads,
 99 and this phenomenon has also been detected exper-
 100 imentally in [17] using speech recordings, in [18] us-
 101 ing simultaneous recordings of laryngeal endoscopy,
 102 acoustics, aerodynamics, electroglottography, and ac-
 103 celeration sensors, and in [19] using simultaneous
 104 speech, electroglottography and accelerometer record-
 105 ings combined with separate resonance estimation
 106 measurements.

107 Although the existence of these perturbations has
 108 been well reported, speech modelling studies have
 109 given only limited attention to the time-domain dy-
 110 namics of fundamental frequency glides where such
 111 perturbations would be expected to occur. Of the
 112 above mentioned studies, upward glides were simu-
 113 lated in [11] by varying the natural frequency of their
 114 physical model over time. Their small amplitude
 115 oscillation model exhibited a frequency jump when
 116 crossing the resonance of their downstream tube when
 117 the acoustic coupling was sufficiently strong. Down-
 118 ward glides were simulated in [14] followed by upward
 119 glides by varying the parameters of a multi-mass vo-
 120 cal fold model. Frequency jumps, subharmonics and
 121 amplitude changes were observed in the regions where
 122 load reactances were changing rapidly. Changes in the
 123 rate of change of the fundamental frequency in these
 124 regions can also be seen in their Figures 10-14. In [16]
 125 upward glides were simulated followed by downward
 126 glides by adjusting the tension parameter (i.e., de-
 127 creasing masses and increasing stiffness parameters by
 128 the same factor) in their four-mass vocal fold model.
 129 They observed frequency jumps associated with reg-
 130 ister changes, which in turn were shown to occur at
 131 different frequencies depending on the VT load.

132 Some of the most popular approaches to modelling
 133 phonation are based on the Kelly-Lochbaum VT [20]
 134 or various transmission line analogues [21, 22, 23].
 135 Contrary to these approaches, the proposed model
 136 consists of (ordinary and partial) differential equa-

tions, conservation laws, and coupling equations. In
 this modelling paradigm, the temporal and spatial
 discretisation is conceptually and practically separ-
 ated from the actual mathematical model of speech.
 The computational model is simply a numerical solver
 for the model equations, written in MATLAB environ-
 ment. The modular design makes it easy to decou-
 ple model components for assessing their significance
 to simulated behaviour.² Since the generalised Web-
 ster’s equation for the VT acoustics assumes intersec-
 tional area functions as its geometric data, VT config-
 urations from magnetic resonance imaging (MRI) can
 be used without transcription to non-geometric model
 parameters. Further advantages of speech modelling
 with Webster’s equation have been explained in [25].

The proposed model is of low order: it aims at qual-
 itatively realistic functionality, tunability by a low
 number of parameters, and tractability of model com-
 ponents, equations, and their relation to biophysics.
 Similar functionality in higher precision can be ob-
 tained using computational fluid dynamics with elas-
 tic tissue boundaries. Such approaches aim to model
 the speech apparatus as undivided whole [26], but the
 computational cost is much higher compared to our
 model or the models proposed in, e.g., [25] and [27].
 Numerical efficiency is a key issue because some pa-
 rameter values or their feasible ranges (in particular,
 for hard-to-get physiological parameters) can only be
 determined by trial and error, leading to a high num-
 ber of required simulations as discussed in [30, Chap-
 ter 4]. The proposed model is hence suitable for in-
 vestigating speech phenomena where realistic model
 output is only produced with a narrow range of con-
 trol parameter values.

2 Phonation Model

2.1 Vocal Fold Mechanics

Voiced speech sounds originate from self-sustained
 quasi-periodic oscillations of the vocal folds where the
 closure of the aperture between the vocal folds, i.e.
 the glottis, cuts off the airflow from lungs in a process
 called phonation. A single period of the glottal flow
 produced by phonation is known as a glottal pulse.

The main mechanism controlling the f_o of voiced
 speech is contraction of the cricothyroid muscles
 which leads to stretching the vocal folds and hence
 increased stress. Secondary mechanisms of f_o control
 include the vertical movement of larynx and changes
 in the subglottal pressure through the control of res-
 piratory muscles.

²Some economy of modelled features is desirable to prevent
 “overfitting” while explaining experimental facts. Good mod-
 elling practices in mathematical acoustics have been discussed
 in [24, Chapter 8].

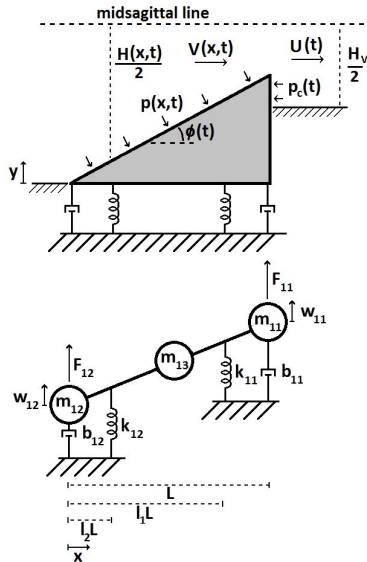


Figure 1: Top: The geometry of the glottis model with the trachea to the left and the vocal tract to the right. Bottom: Lumped-element representation of the lower vocal fold ($j = 1$) with two degrees of freedom.

2.1.1 Equations of motion

The anatomic vocal fold configuration is idealised as a low-order mass-spring system with aerodynamic surfaces as shown in Figure 1. For previous uses and more details on this model, see [28, 29, 30] and [31]. Such lumped-element models have been used frequently (see, e.g., [13, 32, 33, 34, 35, 36] and the reviews [37, 38]) since the introduction of the classic two-mass model [8].

The radically simplified glottis geometry in Figure 1 (top) corresponds to the coronal section through the center of the vocal folds. Both f_o and the phonation type can be changed by adjusting parameter values [30, Section 4]. However, register shifts are not within the scope of this model.

The vocal fold model consists of two wedge-shaped moving elements whose distributed mass is reduced to three mass points which, for the j^{th} fold, $j = 1, 2$, are located so that m_{j1} is at $x = L$, m_{j2} at $x = 0$, and m_{j3} at $x = L/2$. Here L denotes the thickness of the vocal fold structures. The masses are calculated so that the reduced system retains the mass, and static and inertial moments of a parabolic vocal fold shape (for details, see [31, p. 14]). Each vocal fold has two degrees of freedom: m_{j1} and m_{j2} can move in the y -direction. Although this causes some distortion to the shape of the wedges, the displacements in the x -direction are small enough that the effect is negligible. The elastic support of the vocal ligament is approximated by two springs at points $x = l_1L$ and $x = l_2L$, and losses caused by internal resistance of the tissues

to movement and deformation is represented by two dampers at points $x = 0$ and $x = L$.

The equations of motion for the vocal folds are

$$\begin{cases} M_1 \ddot{W}_1(t) + B_1 \dot{W}_1(t) + K_1 W_1(t) = F_1(t), \\ M_2 \ddot{W}_2(t) + B_2 \dot{W}_2(t) + K_2 W_2(t) = F_2(t), \end{cases} \quad t \in \mathbb{R}, \quad (1)$$

where $W_j(t) = [w_{j1}(t) \ w_{j2}(t)]^T$ are the displacements of m_{j1} and m_{j2} in the y -direction as shown in Figure 1 (bottom). The load force pair $F_j(t) = [F_{j1}(t) \ F_{j2}(t)]^T$ comprises acoustic pressure forces as well as aerodynamic pressure forces when the glottis is open (equation (9)) and collision forces when the glottis is closed (equation (5)). The mass, damping, and stiffness matrices M_j , B_j , and K_j , respectively, in (1) are

$$M_j = \begin{bmatrix} m_{j1} + \frac{m_{j3}}{4} & \frac{m_{j3}}{4} \\ \frac{m_{j3}}{4} & m_{j2} + \frac{m_{j3}}{4} \end{bmatrix}, \quad B_j = \begin{bmatrix} b_{j1} & 0 \\ 0 & b_{j2} \end{bmatrix},$$

$$\text{and} \quad K_j = \sum_{i=1}^2 k_{ji} \begin{bmatrix} l_i^2 & l_i(1-l_i) \\ l_i(1-l_i) & (1-l_i)^2 \end{bmatrix}. \quad (2)$$

The entries of these matrices have been computed using Lagrangian mechanics. The damping matrices B_j are diagonal since the dampers are located at the end-points of the vocal folds. The model supports asymmetric vocal fold vibrations but for this work, symmetry of left and right vocal folds is imposed by using parameters $M = M_j$, $K = K_j$, and $B = B_j$, $j = 1, 2$, and by setting $F(t) = F_2(t) = -F_1(t)$. As a further simplification, tissue damping is assumed to be uniform everywhere, i.e., $b_i = \beta$ for $i = 1, 2$. The parameters in (2) as well as the load force components in (1) are illustrated in Figure 1.

The gap between the vocal folds is denoted by $H(x, t)$, and in the model geometry (Figure 1 (top))

$$H(x, t) = H_0(t) + \frac{x}{L} (H_L(t) - H_0(t)), \quad x \in [0, L], \quad (3)$$

where inferior glottal gap $H_0(t) = H(0, t)$ and superior glottal gap $H_L(t) = H(L, t)$ are related to (1) through

$$\begin{bmatrix} H_L(t) \\ H_0(t) \end{bmatrix} = W_2(t) - W_1(t) + \begin{bmatrix} g_L \\ g_0 \end{bmatrix}. \quad (4)$$

The rest gap parameters g_0 and g_L correspond to the points $x = 0$ and $x = L$, respectively.

2.1.2 Vocal fold collision

When the glottis is closed (i.e., $H_L(t) < 0$), there is no airflow between the vocal folds and hence no force arising from it affecting the vocal folds. There are, however, nonlinear spring forces with parameter k_H , accounting for the contact force of the vocal folds. They are accompanied by the acoustic counter pressure from the VT and subglottal tract (SGT), denoted

256 by $p_c = p_c(t)$ in (15). Thus, the force pair for equation
257 (1) during glottal closed phase is given by

$$F = F_H = \left[\begin{array}{c} k_H |H_L|^{3/2} - A_{pc} p_c \\ A_{pc} p_c \end{array} \right], \quad \text{for } H_L < 0, \quad (5)$$

258 where the area $A_{pc} = A_{pc}(t)$ is the nominal area on
259 which p_c acts corrected with relative moment arms
260 (see equation (16)).

261 This approach is related to the Hertz impact model
262 that has been used similarly in [32] and [39]. When
263 the glottis is open (i.e., $H_L(t) > 0$), the spring force
264 in (5) is not enabled. Then the load terms in equa-
265 tion (1) are given by $F(t) = F_A(t)$ as introduced in
266 equation (9) in terms of the aerodynamic forces from
267 the glottal flow.

268 2.2 Glottal Flow Aerodynamics

269 The main component of the airflow within the speech
270 apparatus, to which the acoustic component acts as
271 a perturbation, is assumed to be incompressible and
272 one-dimensional, and to satisfy mass conservation and
273 Newton's second law. The flow is also assumed to
274 be lossless everywhere except at the glottal opening.
275 This main glottal flow (volume velocity) component
276 is described by

$$\dot{U}(t) = \frac{1}{I_L} (p_s(t) - R_g(t)U(t)), \quad (6)$$

277 where $p_s(t)$ is the driving stagnation pressure at the
278 lungs whose time variation is assumed to be slow, I_L
279 regulates the inertia of the load air column, and $R_g(t)$
280 represents non-recoverable losses in the glottis.

281 Equation (6) is related to Newton's second law for
282 the air column in motion, and it can be derived (fol-
283 lowing [31, Section 2.2]) from the pressure balance
284 $p_s = p_g + p_a$, where the pressure change from the
285 lungs to the outside space is the sum of the glottal
286 pressure loss p_g and the accelerating pressure p_a of
287 the fluid column in the airways. To obtain an expres-
288 sion for p_a , the power of accelerating an (incompress-
289 ible) fluid column is considered. This power is equal
290 to the derivative of the kinetic energy of the fluid col-
291 umn, yielding $p_a(t)U(t) = \rho U(t)\dot{U}(t) \int \frac{d\vec{r}}{A(\vec{r})^2}$, where
292 the integration is extended over the VT and SGT vol-
293 umes. Here, $A(\vec{r})$ denotes the area of the fluid column
294 cross-section that contains the position vector \vec{r} , and
295 incompressibility $A(\vec{r})v(\vec{r}, t) = U(t)$ was used. By de-
296 noting the nominal value of inertance $I_L = \rho \int \frac{d\vec{r}}{A(\vec{r})^2}$,
297 these equations yield $p_a = I_L \dot{U}(t)$. In the context
298 of the airways, the nominal inertance can be split
299 into VT and SGT contributions $I_V = \rho \int_0^{L_{VT}} \frac{ds}{A(s)}$ and
300 $I_S = \rho \int_0^{L_S} \frac{ds}{A_S(s)}$, respectively, so that $I_L = I_V + I_S$;
301 see Sections 2.3 and 2.4.

302 Unfortunately, the integration over the volume of
303 airways (even if the SGT geometry was available) does

not necessarily yield the correct total inertance. The
flow outside of mouth as well as the masses of the
lungs, diaphragm, etc., are coupled to the flow. For
the same reason, the inertial effect for VT and SGT,
observed in the low frequency limit of the acoustic
equations (10) and (14), does not give a sufficient ac-
count of the total intertance since not all of it is due to
acoustics. Thus, the inertance parameter I_L must, in
general, be used as a tuning parameter. The high fre-
quency feedback from the VT acoustics to the glottal
flow, a particularly notable effect in phonations where
the glottis does not fully close, is not included in (6).

The glottal pressure loss consists of two components
following [40]

$$p_g = R_g(t)U(t) = \frac{12\mu L_g U(t)}{h H_L(t)^3} + \frac{k_g \rho U(t)^2}{2h^2 H_L(t)^2}. \quad (7)$$

The first term represents the viscous pressure loss,
and it is motivated by the Hagen–Poiseuille law in a
narrow aperture. It approximates the pressure loss in
the glottis using a rectangular tube of width h , height
 H_L , and length L_g . The parameter μ is the kinematic
viscosity of air. The second term takes into account
the pressure losses not attributable to viscosity in the
same sense as the first. The coefficient k_g represents
the difference between pressure drop at the glottal
inlet and recovery at the outlet. This coefficient de-
pends not only on the glottal geometry but also on the
glottal opening, driving pressure, and flow through
the glottis [41]. Equations (6)–(7) bear resemblance
to the description of airflow in [12, 13] where the pres-
sure drop, loss, and recovery effects, however, are ac-
counted for by flow separation in a diverging channel.

The pressure $p(x, t)$ in the glottis is given in terms
of $U = U(t)$ by making use of the Bernoulli theo-
rem $p(x, t) + \frac{1}{2}\rho V(x, t)^2 = p_s$ for the Venturi effect,
where $V(x, t)$ is the velocity within the glottis, and the
mass conservation law $hH(x, t)V(x, t) = U(t)$. Since
each vocal fold has two degrees of freedom, $p(x, t)$ and
the VT/SGT counter pressure p_c can be reduced to
an aerodynamic force pair $F_A = [F_{A,1} \ F_{A,2}]^T$ where
 $F_{A,1}$ acts at $x = L$ and $F_{A,2}$ at $x = 0$ in Figure 1
(bottom). This reduction can be carried out by using
the total force and moment balance equations

$$\begin{aligned} F_{A,1} + F_{A,2} &= h \int_0^L (p(x, t) - p_r) dx \quad \text{and} \\ LF_{A,1} &= \frac{h}{\cos^2 \phi} \int_0^L x(p(x, t) - p_r) dx - LA_{pc} p_c, \end{aligned} \quad (8)$$

where $\phi = \phi(t)$ is the angle of the inclined vocal fold
surface as shown in Figure 1 (top), A_{pc} accounts for
the moment arms and areas on which p_c acts (see
equation (16)), and p_r is the reference pressure cor-
responding to the equilibrium position $w_{ij} = 0$ for
 $i, j = 1, 2$. Since the displacements w_{ij} are in the y -
direction only, the aerodynamic forces have been as-
sumed to act in this direction as well. The moment is

evaluated with respect to point $(x, y) = (0, 0)$ for the lower fold and $(x, y) = (0, H_0)$ for the upper fold.

The force calculations are done using the pressure difference $p(x, t) - p_r$ so that $F_{A,1}$ and $F_{A,2}$ vanish when $p(x, t) = p_r$ and $p_c = 0$. The reference pressure is associated with the hydrostatic pressure reference level in vibrating tissues, and it is expected to satisfy $p_r \leq p_s$. If $p_r = p_s$ is used, the aerodynamic force always tries to close the glottis. For small flow velocities $V(x, t)$, using $p_r < p_s$ results in the driving pressure p_s pushing the vocal folds open more strongly than the aerodynamic force pulls them close. There is no obvious way to determine the true magnitude of p_r as it is an outcome of dynamic pressure equalisation processes related to p_s and the additional partial pressure due to haemodynamics in tissues. For this work, it is assumed that $p_r = 0.5p_s^0$, where $p_s^0 = p_s(0)$, and the equilibrium gap parameter $g_L > 0$ so that starting simulations with a closed glottis is not necessary.

Evaluation of the integrals in (8) yields, for $H_L > 0$,

$$\begin{aligned}
 F_{A,1} &= \frac{hL}{2 \cos^2 \phi} \left(-\frac{\rho U^2}{h^2 H_L (H_0 - H_L)} \right. \\
 &\quad \left. + \frac{\rho U^2}{h^2 (H_L - H_0)^2} \ln \left(\frac{H_0}{H_L} \right) + (p_s - p_r) \right) \\
 &\quad - A_{pc} p_c, \quad \text{and} \\
 F_{A,2} &= \frac{hL}{2 \cos^2 \phi} \left(\frac{\rho U^2 (H_0 \sin^2 \phi + H_L \cos^2 \phi)}{h^2 H_L H_0 (H_0 - H_L)} \right. \\
 &\quad \left. - \frac{\rho U^2}{h^2 (H_L - H_0)^2} \ln \left(\frac{H_0}{H_L} \right) + \cos(2\phi) (p_s - p_r) \right) \\
 &\quad + A_{pc} p_c.
 \end{aligned} \tag{9}$$

During the glottal closed phase (i.e., when $H_L(t) < 0$), the aerodynamic force (9) is not enabled, and the vocal fold load force is instead given by equation (5).

2.3 Vocal Tract Acoustics

A generalised version of Webster's horn model resonator is used as acoustic loads to represent both the VT and the SGT. It is given by

$$\frac{A(s)}{c^2 \Sigma(s)^2} \frac{\partial^2 \psi}{\partial t^2} + 2\pi\alpha W(s) \frac{\partial \psi}{\partial t} - \frac{\partial}{\partial s} \left(A(s) \frac{\partial \psi}{\partial s} \right) = 0, \tag{10}$$

where c denotes the speed of sound, the parameter $\alpha \geq 0$ regulates the energy dissipation through air/tissue interface, and the solution $\psi = \psi(s, t)$ is the velocity potential of the acoustic field; i.e., $v = -\frac{\partial \psi}{\partial s}$.

Then the sound pressure is given by $p = \rho \frac{\partial \psi}{\partial t}$, where ρ denotes the density of air. The generalised Webster's model for acoustic waveguides has been derived from the wave equation in a tubular domain in [42], its solvability and energy notions have been treated in [43], and the approximation properties in [44].

The generalised Webster's equation (10) is applicable if the VT is approximated as a curved

tube of varying cross-sectional area and length L_{VT} . The three-dimensional centreline $\gamma(s)$ of the tube is parametrised using distance $s \in [0, L_{VT}]$ from the superior end of the glottis. At every s , the cross-sectional area of the tube perpendicular to the centreline is given by the area function $A(s)$, and the (hydrodynamic) radius of the tube, denoted by $R(s)$, is defined by $A(s) = \pi R(s)^2$. The curvature of the tube is $\kappa(s) = \|\gamma''(s)\|$, and the curvature ratio $\eta(s) = R(s)\kappa(s) < 1$.

The final parameters appearing in (10) are the stretching factor $W(s)$ and the sound speed correction factor $\Sigma(s)$ for curvature, defined by

$$\begin{aligned}
 W(s) &= R(s) \sqrt{R'(s)^2 + (\eta(s) - 1)^2}, \quad \text{and} \\
 \Sigma(s) &= \left(1 + \frac{1}{4} \eta(s)^2 \right)^{-1/2}.
 \end{aligned} \tag{11}$$

2.3.1 Boundary conditions

The VT resonator is coupled to the glottal flow given by equation (6) with

$$\frac{\partial \psi}{\partial s}(0, t) = -\frac{U_{AC}(t)}{A(0)}, \tag{12}$$

where the DC component has been removed from the glottal flow, i.e., $U_{AC}(t) = U(t) - \frac{1}{T} \int_{t-T}^t U(\tau) d\tau$ with $T = 2/f_0$. The effect of this removal is negligible when phonation has become stable, but it is more pronounced at the beginning of simulations when a stable waveform has not yet developed. Equations (10)–(12) characterise a variant of the source-filter model in the sense that the acoustics of the VT is only excited at the glottis.

At the lips, the reactive acoustic response of the exterior space is modelled by the differential equation

$$\begin{aligned}
 &-R_m L_m \frac{\partial \psi}{\partial s}(L_{VT}, t) \\
 &= \frac{\rho}{A(L_{VT})} \left(R_m \psi(L_{VT}, t) + L_m \frac{\partial \psi}{\partial s}(L_{VT}, t) \right),
 \end{aligned} \tag{13}$$

which corresponds to the impedance $Z(\xi) = \frac{\xi R_m L_m}{R_m + \xi L_m}$ of the same form as the ‘‘first-order high pass model’’ for termination of an acoustic horn in [45, Section 4.1]. The circuit topology of this model is the parallel coupling of a resistor and an inductor.

2.4 Subglottal acoustics

Anatomically, the SGT consists of the airways below the larynx: trachea, bronchi, bronchioles, alveolar ducts, alveolar sacs, and alveoli. This system has been modelled either as a tree-like structure [27] or, more simply, as an acoustic horn whose area increases towards the lungs [34, 46]. We take the latter approach and denote the cross-sectional area and the horn radius by $A_S(s)$ and $R_S(s)$ (see equation (17)),

433 respectively, where $s \in [0, L_S]$ and L_S is the nominal
434 length of the SGT.

435 Since the subglottal horn is assumed to be
436 straight, we have $\eta = 0$, $\Sigma = 1$ and $W_s(s) =$
437 $R_S(s)\sqrt{R'_S(s)^2 + 1}$. Then equations (10)–(12) trans-
438 late to

$$\begin{cases} \frac{A_S(s)}{c^2} \frac{\partial^2 \tilde{\psi}}{\partial t^2} + 2\pi\alpha W_s(s) \frac{\partial \tilde{\psi}}{\partial t} - \frac{\partial}{\partial s} \left(A_S(s) \frac{\partial \tilde{\psi}}{\partial s} \right) = 0, \\ \frac{\partial \tilde{\psi}}{\partial t}(L_S, t) + \theta_s c \frac{\partial \tilde{\psi}}{\partial s}(L_S, t) = 0, \\ \frac{\partial \tilde{\psi}}{\partial s}(0, t) = \frac{U_{AC}(t)}{A_S(0)}, \end{cases} \quad (14)$$

439 where the solution $\tilde{\psi}$ is the velocity potential for the
440 SGT acoustics. Instead of using the reactive bound-
441 ary dynamics (13), the termination loss at lungs is
442 characterised by normalised acoustic resistance $\theta_s \geq 0$
443 in equation (14). SGT acoustics is an important factor
444 in phonation in general but its contribution to changes
445 occurring during glide simulations is negligible as long
446 as f_o is far from the subglottal resonances.

447 2.5 Acoustic counter pressure

448 The feedback coupling from VT/SGT acoustics back
449 to vocal fold surfaces is realised as the product of the
450 acoustic counter pressure $p_c = p_c(t)$ and the moment
451 corrected area $A_{pc} = A_{pc}(t)$ as already shown in equa-
452 tions (5) and (9) above.

453 The counter pressure is the resultant of VT and
454 SGT pressure components, and it is given in terms of
455 velocity potentials from equations (10) and (14) by

$$p_c(t) = Q_{pc}\rho \left(\psi_t(0, t) - \tilde{\psi}_t(0, t) \right), \quad (15)$$

456 where tuning parameter $Q_{pc} \in [0, 1]$ enables scaling
457 the magnitude of the feedback. The parameter Q_{pc} is
458 necessary because the wedge geometry tends to over-
459 estimate the area of the vocal fold surface on which
460 p_c can do work, and further, it is difficult to directly
461 estimate the proportions of the underlying flow and
462 the superimposed acoustics. In simulations, overesti-
463 mation of the acoustic feedback forces leads to perma-
464 nently non-stationary, even chaotic vibrations of the
465 vocal folds, which are outside the scope of this work.

466 The area A_{pc} is best understood in reference to the
467 moment balance in equation (8), although it appears
468 in the same way in both equations (5) and (9). For
469 each vocal fold, p_c acts on the area $\frac{1}{2}(H_V - H_L)h$ and
470 produces a moment arm of $\frac{1}{4}(2H_0 - H_V - H_L)$ around
471 points $(x, y) = (0, 0)$ and $(x, y) = (0, H_0)$ for the lower
472 and upper folds, respectively. Hence

$$A_{pc} = \frac{h}{8L}(H_V - H_L)(2H_0 - H_V - H_L). \quad (16)$$

473 Equations (15) and (16) assume that both the VT
474 and SGT pressure components act in the x -direction
475 only (i.e., horizontally in Figure 1 (top)). This as-
476 sumption minimises the tendency of the wedge geom-
477 etry to overestimate the effect of the SGT compared
478 to the effect of the VT.

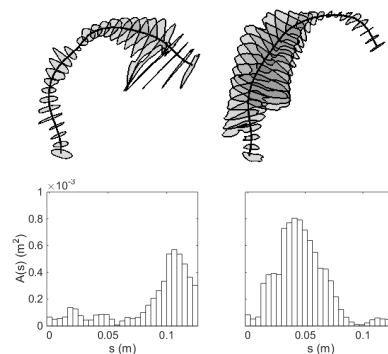


Figure 2: Top: The VT intersections extracted during phonation of [a] and [i]. Bottom: The resulting area functions for equation (10) as a function of distance from the glottis.

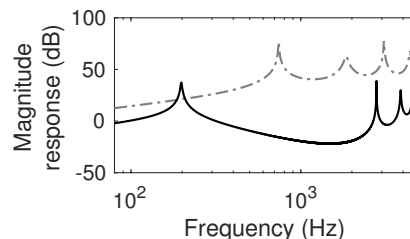


Figure 3: The magnitude responses of the VT acoustic loads obtained by simulating output for an impulse input for [a] (dashed gray) and [i] (solid black). The response of [a] has been raised by 50 dB for clarity.

479 3 Parameters

480 3.1 Vocal tract

Table 1: VT parameter values.

Parameter	[a]	[i]
Inertance, I_V	2540 $\frac{\text{kg}}{\text{m}^4}$	2820 $\frac{\text{kg}}{\text{m}^4}$
Length, L_{VT}	132 mm	136 mm
1 st resonance, f_{R1}	742 Hz	198 Hz
2 nd resonance, f_{R2}	1846 Hz	2791 Hz
Area at mouth	299 mm ²	66 mm ²
R_m	$1.98 \cdot 10^6 \frac{\text{kg}}{\text{s m}^4}$	$8.96 \cdot 10^4 \frac{\text{kg}}{\text{s m}^4}$
L_m	$33.2 \frac{\text{kg}}{\text{m}^4}$	$70.6 \frac{\text{kg}}{\text{m}^4}$
$\text{Re}(Z(400\pi i))$	879	$4.44 \cdot 10^4$
$\text{Im}(Z(400\pi i))$	$4.17 \cdot 10^4$	$4.48 \cdot 10^4$

481 Solving Webster’s equation requires that the VT is
482 represented with an area function and a centreline,
483 from which curvature information can be computed.
484 Two different VT geometries corresponding to vowel-
485 s from a healthy 26 years old female are used: A
486 prolonged [a] produced at $f_o = 168$ Hz and similarly
487 produced [i] at $f_o = 210$ Hz. These geometries have
488 been obtained by MRI using the experimental setting
489 described in [47]; see also [48, 49, 50] for earlier ap-

490 proaches. The extraction of the computational geom-
 491 etry from raw MRI data has been carried out by the
 492 custom software described in [51, 52]. The VT geom-
 493 etries and their area functions are shown in Figure 2,
 494 their simulated frequency responses in Figure 3, and
 495 and the VT geometry dependent parameter values are
 496 given in Table 1.

497 The reactive acoustic loading (13) at the lips re-
 498 quires values for R_m and L_m . The values in Table 1
 499 were obtained by interpolation at 200 Hz from the
 500 piston model given in [53, Chapter 7, Eq. (7.4.31)]
 501 and tuning of R_m to remove excessive fluctuations in
 502 simulated waveforms. The low order rational model
 503 $Z(\xi) = \frac{\xi R_m L_m}{R_m + \xi L_m}$ approximates the irrational piston
 504 model impedance very well for frequencies within
 505 100 Hz . . . 2 kHz, and the frequency responses in Fig-
 506 ure 3 are reasonable as well.

507 3.2 Subglottal tract

508 Full SGT geometry cannot be constructed from the
 509 MRI data that is used for the VT. Instead, an ex-
 510 ponential horn is used as the SGT area function for
 511 equation (14)

$$A_S(s) = A_S(0)e^{\epsilon s}, \text{ where } \epsilon = \frac{1}{L_S} \ln \left(\frac{A_S(L_S)}{A_S(0)} \right) \quad (17)$$

512 following [46]. The values for $A_S(0) = 2 \text{ cm}^2$ and
 513 $A_S(L_S) = 10 \text{ cm}^2$ are taken from [46, Figure 1]. The
 514 horn length L_S is selected so that the lowest subglot-
 515 tal resonance is $f'_{R1} = 500 \text{ Hz}$ which results in the
 516 second lowest resonance at $f'_{R2} = 1.0 \text{ kHz}$. This is a
 517 reasonable value for f_{R1} based on [9, Table 1]; see also
 518 [39, 54, 55] and [27, Figure 1]. The SGT lung termi-
 519 nation resistance in equation (14) is given the value
 520 $\theta_s = 1$ which corresponds to an absorbing boundary
 521 condition. The air column in this SGT model has a
 522 inertia parameter value $I_S = 1040 \text{ kg/m}^4$.

523 3.3 Static parameter values

524 Table 2 lists the numerical values of physiological and
 525 physical constants used in all simulations. Note that
 526 the vocal fold springs are, for this study, placed sym-
 527 metrically about the midpoint of the vocal folds.

528 The masses in M are calculated by combining the
 529 vocal fold shape function used in [32] with female vo-
 530 cal fold length reported in [56], yielding a total vi-
 531 brating mass $m_1 + m_2 + m_3 = 0.27 \text{ g}$. A first estimate
 532 for the spring coefficients in K is calculated by as-
 533 suming that the first eigenfrequency of the vocal folds
 534 matches the starting frequency for the simulations.
 535 The spring coefficients are then adjusted until simu-
 536 lations produce $f_o \approx 145 \text{ Hz}$, giving the initial K^0
 537 for equations (18)–(19) with total spring coefficients
 538 $k_1 + k_2 = 248 \text{ N/m}$. For details of these calculations,
 539 see [31] and [30].

540 The vocal fold damping parameter β plays an im-
 541 portant but problematic role in vocal fold models.

Table 2: Physical and physiological constants.

Parameter	Value
speed of sound in air, c	343 $\frac{\text{m}}{\text{s}}$
density of air, ρ	1.2 $\frac{\text{kg}}{\text{m}^3}$
kinematic viscosity of air, μ	18.27 $\frac{\mu\text{N}\cdot\text{s}}{\text{m}^2}$
VT/SGT loss coeff., α	76 $\frac{\mu\text{s}}{\text{m}}$
glottal gap at rest at $x = 0$, g_0	10.9 mm
glottal gap at rest at $x = L$, g_L	0.4 mm
control gap above glottis, H_V	2 mm
vocal fold length [56], h	10 mm
vocal fold thickness [32], L	6.8 mm
1 st vocal fold spring location, l_1	0.85
2 st vocal fold spring location, l_2	0.15
contact spring constant [32], k_H	730 $\frac{\text{N}}{\text{m}^{3/2}}$
viscous thickness, L_g	1.5 mm
SGT length, L_S	350 mm
resistance at lungs, θ_s	1
entrance/exit coeff., k_g	0.6
initial driving pressure, p_s^0	650 Pa

542 If there is too much damping, sustained oscillations
 543 do not occur. Conversely, too low damping causes
 544 instability in simulated vocal fold oscillations. The
 545 magnitude of physically realistic damping in vibrat-
 546 ing tissues is not available, and, due to its simpli-
 547 fications, the present model could fail to produce
 548 quasi-stationary phonation even if realistic experi-
 549 mental damping values were used. For this article,
 550 $\beta = 0.009 \text{ kg/s}$ is used as it produces slowly changing
 551 glottal pulse amplitudes when simulations are carried
 552 out with constants parameters as well as in feedback
 553 free glides. This damping is small enough that the
 554 resonances of the mass-spring-damper system (1) are
 555 defined approximately by M and K alone.

556 In this work, the nominal values of I_V and I_S , given
 557 in Table 1 and Section 3.2, are used without tuning.

558 4 Computational Aspects

559 4.1 Production of pitch glides

560 The f_o -glides are simulated by controlling two param-
 561 eter values dynamically. First, the matrix K is scaled
 562 while keeping the matrix M constant as the relative
 563 magnitudes of M and K essentially determine the re-
 564 sonance frequencies of vocal fold model (1). This ap-
 565 proach is based on the assumption that the vibrating
 566 mass and the length of the vocal folds are not signif-
 567 icantly changed when the speaker's pitch increases; a
 568 reasonable simplification as far as the frequency range
 569 is small and register changes are excluded.

570 The driving pressure p_s is the second parameter
 571 used to control the glide. The dependence of f_o on
 572 p_s has been observed in simulations [8, 57], physical
 573 experiments using upscaled replicas [12], as well as in
 574 humans [58] and excised canine larynges [59]. The

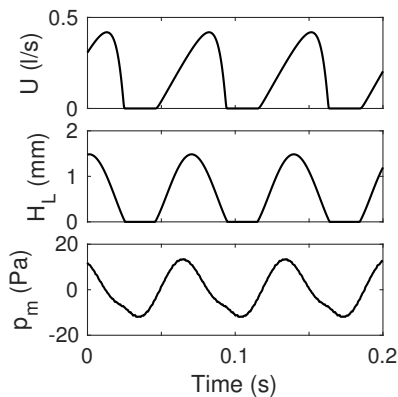


Figure 4: Simulated pulse shapes for [i] with feedback ($Q_{pc} = 0.1$) before the glide begins: glottal flow U , glottal gap H_L , and sound pressure at the lips p_m .

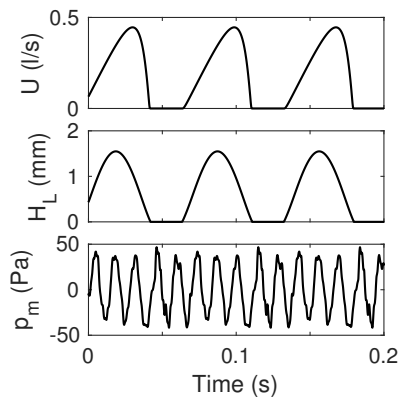


Figure 5: Simulated pulse shapes for [a] with feedback ($Q_{pc} = 0.1$) before glide: glottal flow U , glottal gap H_L , and sound pressure at the lips p_m .

575 impact of p_s on f_o is, however, secondary in these
 576 glides (the f_o trajectories with and without p_s control
 577 differ by at most 10%). Instead, p_s is scaled in order
 578 to maintain phonation and to prevent large changes
 579 in phonation type as the stiffness of the vocal folds
 580 changes. It was found by trial and error, that equal
 581 scaling of p_s and K best maintained the glottal open
 582 quotient OQ (proportion of glottal cycle during which
 583 the glottis is open, see [60, Figure 4]), the closing
 584 quotient CIQ (proportion of the glottal cycle during
 585 which the flow is decreasing), and the maximum of
 586 H_L approximately steady over the upward glide when
 587 acoustic feedback was disabled.

588 The parameters are scaled exponentially with time

$$K(t) = 2.2^{2t/T} K^0, \quad p_s(t) = 2.2^{t/T} p_s^0 \quad (18)$$

589 for rising glides, and

$$K(t) = 2.2^{2-2t/T} K^0, \quad p_s(t) = 2.2^{1-t/T} p_s^0 \quad (19)$$

590 for falling glides. The duration of the glide is $T = 3$ s,
 591 and t is the time from the beginning of the glide. Note
 592 that the temporal scale of the glides is long compared
 593 to glottal cycles, and hence the control parameters K
 594 and p_s can be regarded as static from the point of view
 595 of the vocal fold dynamics. Other starting conditions
 596 (particularly, vocal fold displacements and velocities,
 597 and pressure and velocity distributions in the resonators)
 598 are taken from stabilised simulations. These
 599 parameters produce glides with f_o approximately in
 600 the range [145 Hz, 315 Hz], although the exact range
 601 depends on the VT geometry and feedback level.

602 4.2 Numerical realisation

603 The model equations are solved numerically using
 604 MATLAB software and custom-made code. The vocal
 605 fold equations of motion (1) are solved by the
 606 fourth order Runge–Kutta time discretisation scheme.
 607 The flow equation (6) is solved by the backward Euler
 608 method. The VT and SGT are discretised by

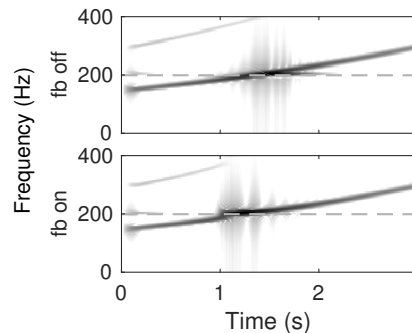


Figure 6: Spectrogram of pressure at lips during glide for [i]. Top: without feedback ($Q_{pc} = 0$). Bottom: with feedback ($Q_{pc} = 0.1$). Dashed gray line is f_{R1} .

609 FEM using piecewise linear elements ($N = 29$ for
 610 VT and $N = 10$ for SGT) and the physical energy
 611 norm of Webster’s equation. Energy preserving
 612 Crank–Nicolson time discretisation (i.e., Tustin’s
 613 method [61]) is used for the resonators. The time
 614 step is generally $10 \mu\text{s}$ which is small enough to keep
 615 the frequency warping in Tustin’s method under one
 616 semitone for frequencies under 13 kHz. Reduced time
 617 step, however, is used near glottal closure. This is
 618 due to the discontinuity in the aerodynamic force (9)
 619 at the closure which requires numerical treatment by
 620 interpolation and time step reduction as explained in
 621 [31, Section 2.4.1].

622 Solving the equations of motion of the vocal folds
 623 is the computationally most expensive part of the
 624 model, taking approximately 55% of the running time
 625 in simulations of steady phonation with constant
 626 parameter values. In comparison, solving the Web-
 627 ster’s equations with precomputed mass, stiffness, and
 628 damping matrices takes approximately 10% of the
 629 simulation time, and the flow equation solver less than
 630 2%. Simulation of 1 s takes approximately 20 s on a
 631 standard professional desktop computer.

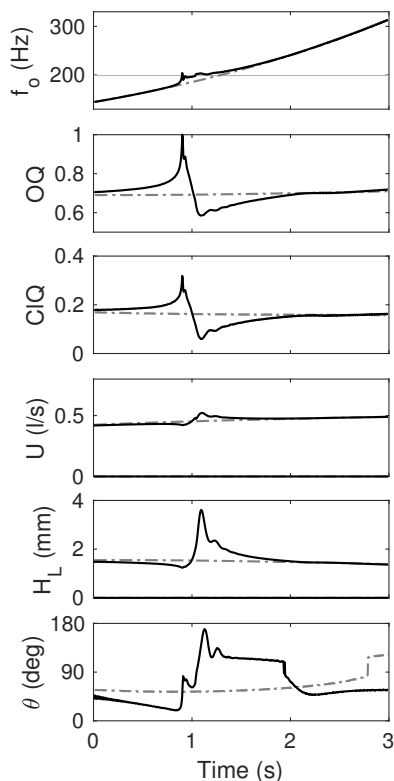


Figure 7: Glide for [i] with feedback ($Q_{pc} = 0.1$) (solid black) and without feedback ($Q_{pc} = 0$) (dashed gray). Shown are fundamental frequency f_o (horizontal gray line is f_{R1}), open quotient OQ , closing quotient ClQ , envelopes of glottal flow U and gap H_L , and phase difference θ between m_{j1} and m_{j2} .

5 Simulation Results

The glottal flow U and gap H_L (or more generally the glottal area hH_L) pulses produced by the model (Figures 4–5) appear realistic when compared to the experimental data presented in [54, Figures 4–7], the signals produced by different numerical models (see [8, Figures 14a–14c], [27, Figures 10–11], [39, Figures 8 and 10], [62, Figure 6], [63, Figure 5]), and the glottal pulse waveforms obtained by inverse filtering in, e.g., [64, Figures 10–13], [60, Figures 3 and 6], and [65, Figures 5.3, 5.4, and 5.17]. Quantitative comparison of the model to the LF model can be found in [66]. The skewing of U relative to H_L – an effect that has been observed in natural speech, e.g., with the help of inverse filtering in [67, 68] – is mainly produced by the inertial term in (6).

The results of upward glide simulations for [i] are shown in Figures 6–7. Figure 6 displays spectrograms of the sound pressure signal at the lips with and without feedback. For Figure 7, the f_o trajectory, OQ , and ClQ have been extracted from U pulse by pulse. Envelopes of U , and H_L are also displayed, and the phase difference θ between m_{j1} and m_{j2} has been es-

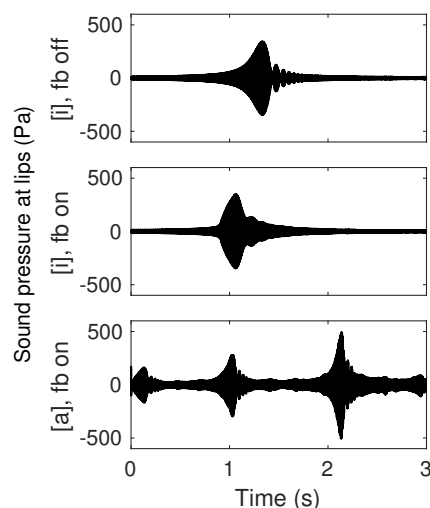


Figure 8: Sound pressures at the lips during upward glides. Top: [i] without feedback ($Q_{pc} = 0$). Middle: [i] with feedback ($Q_{pc} = 0.1$). Bottom: [a] with feedback ($Q_{pc} = 0.1$).

timated based on how much peaks in H_0 are delayed compared to H_L .

The simulations indicate a consistent locking pattern in f_o trajectories at $f_{R1}[i]$ which vanishes if the VT feedback is decoupled by setting $Q_{pc} = 0$. This locking pattern for rising glides can be seen in Figure 6 as a discontinuity in the f_o contour near f_{R1} followed by an interval where f_o appears to be approximately constant. More details are visible in the f_o trajectory in Figure 7: a rapid rise in f_o (hereafter referred to as a jump), a locking to a plateau at approximately f_{R1} , and a smooth release. The height of the jump, degree of overshoot and oscillations about the plateau level, as well as the duration of the locking event depend on parameter choices (see, e.g., Figure 11). In the glide displayed in Figure 7, the f_o trajectories deviate by over 1% in the range 178–215 Hz as measured from feedback free trajectory, and the overshoot at the frequency jump reaches 205 Hz. The flattest part of the locking, which follows the overshoot, occurs at 195–197 Hz.

The frequency jump in the simulations is preceded by a decrease in vocal fold oscillation and glottal flow amplitudes (Figure 7), and a decrease in the phase difference between upper and lower vocal fold masses. This is accompanied by increased breathiness in the phonation, as characterised by increasing OQ and ClQ values, which reduces the effect of the feedback from the acoustics to the vocal folds. The locking plateau coincides with a nearly constant rate of decreasing OQ and ClQ , and increasing amplitude of, in particular, H_L . At the same time, there are large but smooth changes in θ . After the release of f_o the glottal pulse characteristics return gradually to the feedback free trajectories, except for θ . The sudden

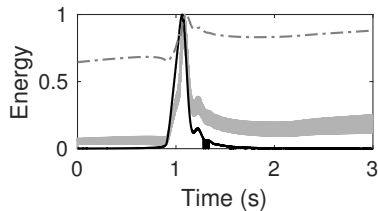


Figure 9: Normalised envelope of energy in VT acoustics (solid black) and in the glottal flow U (dashed gray), and energy in vocal fold vibrations (solid gray) in upward glide for [i] with $Q_{pc} = 0.1$.

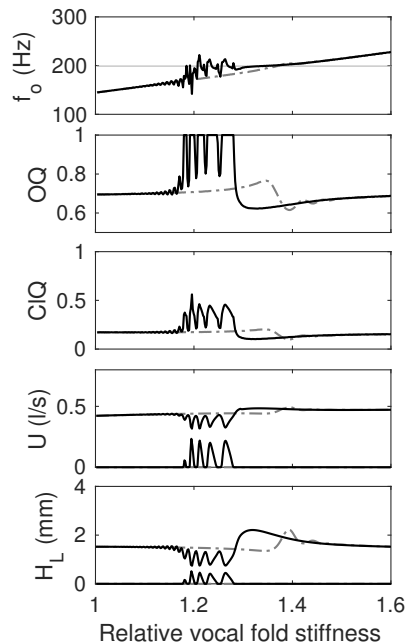


Figure 10: Upward (dashed gray) and downward (solid black) glides for vowel [i] with $Q_{pc} = 0.04$. Shown are fundamental frequency f_o (f_{R1} indicated by horizontal gray line), open quotient OQ , closing quotient ClQ , and the envelopes of glottal flow U and gap H_L . On the x -axis, relative vocal fold stiffness refers to the coefficient of the K^0 matrix in equations (18) and (19).

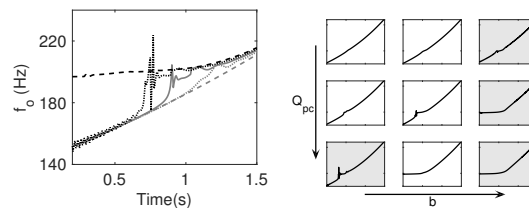


Figure 11: Left: f_o trajectories for [i] with different values of Q_{pc} : gray dashed 0.0, gray dotted 0.05, gray solid 0.1, black dotted 0.15, and black dashed 0.2. Right: f_o trajectories for [i] qualitatively as Q_{pc} and β increase in the direction of the arrow. Light gray background indicates that small parameter changes can lead to loss of quasi-stable glides.

690 changes in θ seen at 1.9 s with feedback and at 2.8 s
 691 without feedback are caused by the method of esti-
 692 mating θ . Near these instants H_0 pulses have shallow
 693 double peaks, and the sudden change occurs when the
 694 dominant peak shifts from one to the other. Note,
 695 however, that changes in pulse shapes are smooth near
 696 these instants. Further, H_0 and H_L have well defined
 697 single peaks at and near the locking event, so changes
 698 in θ there are not caused by this same phenomenon.

699 This locking behaviour of f_o or the related wave-
 700 form changes are not observed for glides of [a] where
 701 $f_{R1}[a]$ is not inside the simulated frequency range
 702 [145 Hz, 315 Hz]. The differences in the f_o trajec-
 703 tories and glottal pulse characteristics between feedback
 704 ($Q_{pc} = 0.1$) and feedback free ($Q_{pc} = 0$) confi-
 705 gurations are negligible for [a].

706 The VT resonance $f_{R1}[i]$ and the resonance frac-
 707 tions $f_{R1}[a]/5 = 148$ Hz, $f_{R1}[a]/4 = 186$ Hz and
 708 $f_{R1}[a]/3 = 247$ Hz are within the frequency range,
 709 and the corresponding events are visible in the sound
 710 pressure signal at the lips (Figure 8). Note that de-
 711 spite this visibility, corresponding events can be seen
 712 in the glottis only for the event in the middle panel,
 713 i.e. $f_{R1}[i]$ with feedback. For [a], the pressure sig-
 714 nals with and without feedback are nearly identical (only
 715 glide with feedback is shown in Figure 8). For [i], the
 716 largest difference in the pressures is the timing of the
 717 resonance event.

718 When feedback is disabled, energy cannot be trans-
 719 ferred from the resonating vocal tract to the oscillat-
 720 ing vocal folds or to the glottal flow. Figure 9 shows
 721 how energy, normalised to one, in each of the subsys-
 722 tems develops when feedback is on. As the resonance
 723 nears, p_c does work on the vocal folds increasing the
 724 energy in the vocal fold oscillations which in turn feeds
 725 energy into U . Since p_c has an increasingly strong pe-
 726 riodic component at $f_{R1}[i]$, all three subsystems get
 727 locked to this frequency. Unlocking occurs when the
 728 first vocal fold eigenfrequency has been raised suffi-
 729 ciently for the energy in the oscillations to win out
 730 over the frequency of p_c .

731 Rising and falling glides show different perturba-
 732 tion patterns as shown in Figure 10. The x -axis in
 733 this figure is the relative vocal fold stiffness, which for
 734 rising glides is $2.2^{t/T}$ and for falling glides $2.2^{1-t/T}$

735 as given in equations (18) and (19). For given model
 736 parameter values, falling glides exhibit more fluctua-
 737 tions in glottal pulse parameters at the locking event
 738 and the perturbation lasts longer. The fluctuations in
 739 f_o in the falling glides during the locking and at fre-
 740 quencies below this are qualitatively similar to what
 741 occurs at extreme values of Q_{pc} and β for rising glides.

742 The feedback parameter Q_{pc} plays, unsurprisingly,
 743 a key role in the f_o jump and locking in glides for
 744 [i] as shown in Figure 11 (left). With no acoustic
 745 feedback to the vocal folds, there are no perturbations

in f_o , whereas with a high Q_{pc} , starting a glide with f_o below f_{R1} is not possible without decreasing K^0 . If a starting f_o below f_{R1} is obtainable, a high Q_{pc} value results in a large overshoot at the jump, and fluctuations in f_o both before the jump and at the beginning of the plateau.

Besides Q_{pc} , the locking pattern is also sensitive to other model parameters, in particular the vocal fold damping β . In fact, β and Q_{pc} affect the locking behaviour in complementary ways, as qualitatively shown in Figure 11 (right). The full frequency range [145 Hz, 315 Hz] for f_o can be obtained with modal locking if $Q_{pc} \in [0.05, 0.12]$ and $\beta \in [0.005, 0.015]$. Beyond these ranges, an increase in one parameter needs to be compensated for with a decrease in the other. Otherwise, the locking pattern disappears or the simulated f_o range is reduced to above $f_{R1}[i]$.

The stability of glide simulations (understood as slowly changing amplitude envelope of glottal flow U) becomes a serious issue at high values of one or both of the parameters Q_{pc} and β . The driving pressure p_s in glide simulations is dynamically controlled as given in equations (18)–(19). If p_s were instead kept constant, we would observe an increasing OQ and decreasing amplitudes of glottal flow and vocal fold oscillations throughout the glide but the qualitative behaviour of modal locking events, including the behaviour of phonation type parameters around these events, would remain very similar.

6 Discussion

We have reported observations on the locking of f_o at a resonance of the VT in simulated pitch glides. The locking behaviour shows a consistent time-dependent behaviour that is similar for rising and falling glides. The f_o jump at the beginning of the locking in rising glides and end of the locking in falling glides occurs together with and increased breathiness of phonation as characterised by open quotient OQ and closing quotient ClQ . During the locking plateau, these parameters indicated an approximately steady decrease in breathiness.

The locking takes place only at frequencies determined by supraglottal resonances. Use of p_s as a secondary control parameter for the glides ensure that the main cause for changes in OQ and ClQ is the acoustic loading. By modifying the strength of the acoustic feedback (i.e., the parameter Q_{pc} in equation (15)) and vocal fold tissue losses (i.e., the parameter β), the locking tendency at $f_{R1}[i]$ may be modulated from non-existent (where both Q_{pc} and β have low values) to extreme locking at $f_{R1}[i]$ without release (where Q_{pc} and/or β have large values); see Figure 11. Small changes to the model (as discussed below) leave the locking behaviour at $f_{R1}[i]$ unchanged, even though the model parameter values required for the desired glottal waveform change (cf.

[28, 29]). We conclude that the simulation results on vowel glides reported in Section 5 reflect the model behaviour in a consistent and robust manner.

To what extent do the simulation results validate the proposed model? The model produces perturbations of the glottal pulses at VT resonances and, additionally, sound pressure perturbations at some of the VT resonance fractions. Of the former, a wide existing literature was reviewed in Section 1. Observations on perturbations in speech at formant fractions have not been reported, to our knowledge, in experimental literature. There is a particular temporal pattern of locking in simulated perturbations at $f_{R1}[i]$ as shown in Figures 6 and 7 (topmost panel). A similar pattern can be seen in the speech spectrograms given in [17, Figure 5], [16, Figure 4], as well as in the vowel glide samples in the data set of [3]. The pitch trajectory and speech spectrogram in [19, Figure 4] also show locking but no release. A similar locking behaviour can also be interpreted to lie behind the experimental results shown in [12, Figures 10b and 13b], and it also tends to emerge in model simulations even if the acoustic feedback is realised in different manner; see, e.g., [14, Figures 13 and 14] and [69, Figure 6].

6.1 Acoustics

The effect of physically realistic values of parameter α in model simulations is negligible; see [25, Section 5] and [30, Section 3.3.2]. These losses move the VT resonance positions computed from equations (10) slightly. On the other hand, the VT resonances are quite sensitive to the parameters of the parallel RL model in equation (13), similar to the simplified model proposed in [45, Eq. (28)]. In its most general form, the model in [45, Eq. (39)] is an integro-differential delay equation with nine parameters and a single delay lag. Unfortunately, it cannot be introduced to Webster’s model as a boundary condition: this is the salient feature of equation (13) that simplifies the implementation of the FEM solver.

It is expected that the otherwise small subglottal effect in simulations will get more pronounced when $f_o \rightarrow f'_{R1}$, and similarly VT impact for [a] will increase when $f_o \rightarrow f_{R1}[a]$. These resonance frequencies, as well as the fractions $f_{R1}[i]/n$, $n = 2, 3, \dots$, are not included in the glides because the two glide controls appear to be insufficient to maintain phonation through such a large frequency range. Such glides would likely require dynamic control of vocal fold length and mass as well. The similarity of the VT and SGT resonators is visible near the resonance fractions in the presented glides, however: The first subglottal resonance fraction $f'_{R1}/2$ shows up in the counter pressure (15) in the same way as $f_{R1}[a]/n$.

The SGT acoustics model proposed in [27] is likely to produce the correct resonance distribution and frequency-dependent energy dissipation rate at the

lung end without tuning. The horn model requires tuning of the horn geometry in order to get the lowest subglottal resonance realistic $f'_{R1} = 500$ Hz. Doing so freezes all the higher subglottal resonances at fixed positions, e.g., $f'_{R2} = 1.0$ kHz. The branching subglottal models given in [27, Figure 8] have the second subglottal resonance between 1.3 kHz and 1.5 kHz. It was observed in [70] that the soft tissues introduce an additional nonacoustic resonance to the subglottal system that is lower than the first subglottal formant f'_{R1} attributed to air column dynamics. There is no obvious way how a horn model could be used to accommodate such a resonance at ca. 350 Hz due to the yielding wall dynamics.

6.2 Vocal folds and glottal flow

The vocal fold geometry shown in Figure 1 (top) leads to a simple expression for the aerodynamic force in equation (9). The further simplification of keeping the direction of $p(x, t)$ constant (i.e., considering changes in ϕ negligible) is possible without affecting the qualitative behaviour of the model. The difference between the driving pressure p_s and the reference pressure p_r can be included in the force balance when the glottis is closed (equation (5)) although the wedge-shaped vocal folds, their point-like collision, and the assumption of incompressible glottal flow lead to overestimation of the effect. This addition causes an increase in the open quotient throughout simulations, but if the model parameters are adjusted to achieve a phonation similar to Figures 4–5 before the glides, the locking behaviour remains qualitatively unchanged.

Replacing the sharp peaks by flat tops in Figure 1 results in phonation that has typically lower open quotient (OQ) compared to the original wedge-like geometry. This change makes it easier to adjust the parametrisation of the model to obtain some phonation targets. In particular, the value of the glottal loss parameter k_g can then be based on experimental values (e.g., [41]) since the model geometry becomes more similar to the experimental model geometry (M5).

The importance of entrance and exit effects represented by k_g can be seen, for example, by comparing simulated volume velocities and glottal areas with the experimental curves in [40, Figure 3], obtained from a physical model of the glottis. In model simulations, leaving out this transglottal pressure loss term changes the glottal pulse waveform significantly if other model parameters are kept the same, as shown in [30, Figure 3.7]. About half of the total pressure loss in simulations is due to entrance and exit effects at the peak of opening of the glottis; see [30, Figure 3.6]. However, the behaviour of the simulated f_o trajectories over $f_{R1}[i]$ does not change if $k_g = 0$. Then, however, the vowel glide must be produced by different model parameter values.

The glottal flow has been studied extensively since 1950's. Compared to the flow model used here, physiologically more faithful glottal flow solvers have been proposed in, e.g., [35, 46, 62, 71, 72] and [73]. As pointed out in [72], more sophisticated flow models are challenging to couple to acoustic resonators since the interface between the flow-mechanical (in particular, the turbulent) and the acoustic components is no longer clearly defined.

Direct feedback from VT acoustics to the glottal flow can be added to the model although it has been left outside the scope of this work. In implementing this feedback mode, particular care must be taken to remove the additional acoustic contribution in the inertial effect, which is already accounted for by (6). The impact of this feedback mechanism is expected to be notable around the f_o jump, when the glottal closure is short or non-existent.

Turbulence in supraglottal space is a spatially distributed acoustic source, and it does not provide a spatially localised acoustic signal for the resonator in equation (12). Much of the turbulence noise energy lies above 4 kHz where Webster's model equation (10) is not an accurate description [74, 75]. The unmodelled supraglottal jet may even exert an additional aerodynamic force to vocal folds that would not be part of the acoustic counter pressure p_c .

7 Conclusions

We have presented a model for vowel production, based on (partial) differential equations, that consists of submodels for glottal flow, vocal folds oscillations, and acoustic responses of the VT and SGT cavities. The model was used for simulations of rising and falling vowel glides of [a, i] in frequencies that span one octave [145 Hz, 315 Hz]. This interval contains the lowest VT resonance f_{R1} of [i] but not that of [a]. Perturbation events in simulated vowel glides were observed at VT acoustic resonances, or at some of their fractions but nowhere else.

The fundamental frequency f_o of the simulated vowel was observed to lock to $f_{R1}[i]$ but similar locking was not seen at any of the resonance fractions of [a]. The locking events were accompanied by changes in the phonation: increased breathiness below and partially at the locking frequency and steady change in breathiness during most of the lock. If these changes can also be detected in glides produced by human speakers, e.g., by using electroglottography, they may provide an indirect means of identifying locking events when coincidence of f_o and f_{R1} makes it challenging to track them both.

The locking event takes place only when the acoustic feedback from VT to vocal folds is present, and then it has a characteristic time-dependent behaviour. A large number of simulation experiments were carried out with different parameter settings of the model

970 to verify the robustness and consistency of all observa-
 971 tions. The similarity between simulated pitch pattern
 972 and experimental results in literature was achieved
 973 by using feedback from acoustics to vocal fold tis-
 974 sues, indicating that this feedback mode can be strong
 975 enough to affect speech outcomes.

976 The simulation model does not include the neural
 977 control actions on the vocal fold structures or dy-
 978 namic modifications of the VT geometry. There is
 979 also a significant control action affecting the driving
 980 stagnation pressure and it has been used as a control
 981 variable in equations (18)–(19) for glide productions.
 982 In humans, neural control actions are part of feedback
 983 loops, of which some are auditive, and some others op-
 984 erate directly through tissue innervation and the cen-
 985 tral nervous system. So little is known about these
 986 feedback mechanisms that their explicit mathemat-
 987 ical modelling seems infeasible. Instead, the model
 988 parameters for simulations are tuned so that the sim-
 989 ulated glottal pulse waveform corresponds to experi-
 990 mental speech data. Despite these simplifications the
 991 model appears to be sufficiently detailed to replicate
 992 the observations found in literature.

993 Acknowledgements

994 This study was funded by the Academy of Finland
 995 (projects no. 284671 and 312490), the Finnish gradu-
 996 ate school in engineering mechanics, Finnish Academy
 997 project Lastu 135005, 128204, and 125940; European
 998 Union grant Simple4All (grant no. 287678), Aalto
 999 Starting Grant 915587, and Åbo Akademi Institute
 1000 of Mathematics. The authors would like to thank the
 1001 four anonymous reviewers in 2013 and 2016 for com-
 1002 ments leading to many improvements of the model.

1003 References

- 1004 [1] T. Chiba, M. Kajiyama: The vowel, its nature and
 1005 structure. Phonetic Society of Japan, Tokyo, 1941.
- 1006 [2] G. Fant: Acoustic theory of speech production. Mou-
 1007 ton, The Hague, 1960.
- 1008 [3] D. Aalto, J. Malinen, M. Vainio, Modal locking be-
 1009 tween vocal fold and vocal tract oscillations: Ex-
 1010 periments and statistical analysis. ArXiv e-prints,
 1011 arXiv:1211.4788, 2016.
- 1012 [4] I. R. Titze, R. J. Baken, K. W. Bozeman,
 1013 S. Granqvist, N. Henrich, C. T. Herbst, D. M.
 1014 Howard, E. J. Hunter, D. Kaelin, R. D. Kent,
 1015 J. Kreiman, M. Kob, A. Löfqvist, S. McCoy, D. G.
 1016 Miller, H. Noé, R. C. Scherer, J. R. Smith, B. H.
 1017 Story, J. G. Švec, S. Ternström, J. Wolfe: Toward a
 1018 consensus on symbolic notation of harmonics, reso-
 1019 nances, and formants in vocalization. The Journal of
 1020 the Acoustical Society of America **137** (2015) 3005–
 1021 3007.
- 1022 [5] P. Alku, J. Horáček, M. Airas, F. Griffond-Boitier,
 1023 A.-M. Laukkanen: Performance of glottal inverse fil-
 1024 tering as tested by aeroelastic modelling of phona-
 1025 tion and FE modelling of vocal tract. Acta Acustica
 1026 united with Acustica **92** (2006) 717–724.
- [6] P. Alku, J. Pohjalainen, M. Vainio, A.-M. Laukka-
 1027 nen, B. H. Story: Formant frequency estimation of
 1028 high-pitched vowels using weighted linear prediction.
 1029 The Journal of the Acoustical Society of America **134**
 1030 (2013) 1295–1313.
- [7] J. Guðnason, D. D. Mehta, T. F. Quatieri: Eval-
 1032 uation of speech inverse filtering techniques using
 1033 a physiologically based synthesizer. Proceedings of
 1034 2015 IEEE International Conference on Acoustics,
 1035 Speech and Signal (ICASSP), April 2015, 4245–4249.
- [8] K. Ishizaka, J. L. Flanagan: Synthesis of voiced
 1037 sounds from a two mass model of the vocal cords.
 1038 Bell System Technical Journal **51** (1972) 1233–1268.
- [9] S. F. Austin, I. R. Titze: The effect of subglottal
 1040 resonance upon vocal fold vibration. Journal of Voice
 1041 **11** (1997) 391–402.
- [10] Z. Zhang, J. Neubauer, D. A. Berry: The influence of
 1043 subglottal acoustics on laboratory models of phona-
 1044 tion. The Journal of the Acoustical Society of Amer-
 1045 ica **120** (2006) 1558–1569.
- [11] J. C. Lucero, K. G. Lourenço, N. Hermant, A. Van
 1047 Hirtum, X. Pelorson: Effect of source-tract acoustical
 1048 coupling on the oscillation onset of the vocal folds.
 1049 The Journal of the Acoustical Society of America **132**
 1050 (2012) 403–411.
- [12] N. Rutu, X. Pelorson, A. Van Hirtum, I. Lopez-
 1052 Arteaga, A. Hirschberg: An in-vitro setup to test
 1053 the relevance and the accuracy of low-order vocal
 1054 folds models. The Journal of the Acoustical Society
 1055 of America **121** (2007) 479–490.
- [13] N. Rutu, X. Pelorson, A. Van Hirtum: Influence
 1057 of acoustic waveguides lengths on self-sustained os-
 1058 cillations: Theoretical prediction and experimental
 1059 validation. The Journal of the Acoustical Society of
 1060 America **123** (2008) 3121–3121.
- [14] I. R. Titze: Nonlinear source-filter coupling in phona-
 1062 tion: Theory. The Journal of the Acoustical Society
 1063 of America **123** (2008) 2733–2749.
- [15] H. Hatzikirou, W. T. Fitch, H. Herzel: Voice instabil-
 1065 ities due to source-tract interactions. Acta Acustica
 1066 united with Acustica **92** (2006) 468–475.
- [16] I. T. Tokuda, M. Zemke, M. Kob, H. Herzel: Biome-
 1068chanical modeling of register transitions and the role
 1069 of vocal tract resonators. The Journal of the Acous-
 1070 tical Society of America **127** (2010) 1528–1536.
- [17] I. R. Titze, T. Riede, P. Popolo: Nonlinear source-
 1072 filter coupling in phonation: Vocal exercises. The
 1073 Journal of the Acoustical Society of America **123**
 1074 (2008) 1902–1915.
- [18] M. Zaňartu, D. D. Mehta, J. C. Ho, G. R. Wodicka,
 1076 R. E. Hillman: Observation and analysis of in vivo
 1077 vocal fold tissue instabilities produced by nonlinear
 1078 source-filter coupling: A case study. The Journal of
 1079 the Acoustical Society of America **129** (2011) 326–
 1080 339.

- 1082 [19] L. Wade, N. Hanna, J. Smith, J. Wolfe: The role of vocal tract and subglottal resonances in producing vocal instabilities. *The Journal of the Acoustical Society of America* **141** (2017) 1546–1559. 1140
- 1083 1141
- 1084 1142
- 1085
- 1086 [20] K. L. Kelly, C. C. Lochbaum: Speech synthesis. Proceedings of the Fourth International Congress on Acoustics, 1962, Paper G42, 1–4. 1143
- 1087 1144
- 1088 1145
- 1089 [21] H. K. Dunn: The calculation of vowel resonances, and an electrical vocal tract. *The Journal of the Acoustical Society of America* **22** (1950) 740–753. 1146
- 1090 1147
- 1091 1148
- 1092 [22] S. El-Masri, X. Pelorson, P. Saguet, P. Badin: Development of the transmission line matrix method in acoustics. Applications to higher modes in the vocal tract and other complex ducts. *International Journal of Numerical Modelling: Electronic Networks, Devices and Fields* **11** (1998) 133–151. 1149
- 1093 1150
- 1094 1151
- 1095 1152
- 1096 [23] J. Mullen, D. Howard, D. Murphy: Waveguide physical modeling of vocal tract acoustics: Flexible formant bandwidth control from increased model dimensionality. *IEEE Transactions on Audio, Speech, and Language Processing* **14** (2006) 964–971. 1153
- 1097 1154
- 1098 1155
- 1099 1156
- 1100 [24] S. Rienstra, A. Hirschberg: An introduction to acoustics. Eindhoven University of Technology, 2013. 1157
- 1101 1158
- 1102 1159
- 1103 [25] K. van den Doel U. M. Ascher: Real-time numerical solution of Webster’s equation on a nonuniform grid. *IEEE Transactions on Audio, Speech, and Language Processing* **16** (2008) 1163–1172. 1160
- 1104 1161
- 1105 1162
- 1106 1163
- 1107 1164
- 1108 1165
- 1109 [26] J. Horáček, V. Uruba, V. Radolf, J. Veselý, V. Bula: Airflow visualization in a model of human glottis near the self-oscillating vocal folds model. *Applied and Computational Mechanics* **5** (2011) 21–28. 1166
- 1110 1167
- 1111 1168
- 1112 1169
- 1113 [27] J. C. Ho, M. Zaňartu, G. R. Wodicka: An anatomically based, time-domain acoustic model of the subglottal system for speech production. *The Journal of the Acoustical Society of America* **129** (2011) 1531–1547. 1170
- 1114 1171
- 1115 1172
- 1116 1173
- 1117 1174
- 1118 [28] T. Murtola, J. Malinen: Waveform patterns in pitch glides near a vocal tract resonance. Proceedings of INTERSPEECH 2017, Stockholm, 2017, 3487–3491. 1175
- 1119 1176
- 1120 1177
- 1121 [29] A. Aalto, T. Murtola, J. Malinen, D. Aalto, M. Vainio: Modal locking between vocal fold and vocal tract oscillations: Simulations in time domain. ArXiv e-prints, arXiv:1506.01395, 2017. 1178
- 1122 1179
- 1123 1180
- 1124 1181
- 1125 [30] T. Murtola: Modelling vowel production. Licentiate thesis, Aalto University School of Science, Espoo, Finland, 2014. 1182
- 1126 1183
- 1127 1184
- 1128 [31] A. Aalto: A low-order glottis model with nonturbulent flow and mechanically coupled acoustic load. Master’s thesis, Helsinki University of Technology, Espoo, Finland, 2009. 1185
- 1129 1186
- 1130 1187
- 1131 1188
- 1132 [32] J. Horáček, P. Šidlof, J. G. Švec: Numerical simulation of self-oscillations of human vocal folds with Hertz model of impact forces. *Journal of Fluids and Structures* **20** (2005) 853–869. 1189
- 1133 1190
- 1134 1191
- 1135 1192
- 1136 [33] J. Liljencrants: A translating and rotating mass model of the vocal folds. *STL-QPSR* **32** (1991) 1–18. 1193
- 1137 1194
- 1138 [34] N. J. C. Lous, G. C. J. Hofmans, R. N. J. Veldhuis, A. Hirschberg: A symmetrical two-mass vocal-fold model coupled to vocal tract and trachea, with application to prosthesis design. *Acta Acustica united with Acustica* **84** (1998) 1135–1150. 1195
- 1139 1196
- 1197 1198
- 1199 [35] X. Pelorson, A. Hirschberg, R. R. van Hassel, A. P. J. Wijnands, Y. Auregan: Theoretical and experimental study of quasisteady-flow separation within the glottis during phonation. Application to a modified two-mass model. *The Journal of the Acoustical Society of America* **96** (1994) 3416–3431. 1199
- 1200 1200
- 1201 [36] B. H. Story, I. R. Titze: Voice simulation with a body-cover model of the vocal folds. *The Journal of the Acoustical Society of America* **97** (1995) 1249–1260. 1201
- 1202 1202
- 1203 [37] B. D. Erath, M. Zaňartu, K. C. Stewart, M. W. Plesniak, D. E. Sommer, S. D. Peterson: A review of lumped-element models of voiced speech. *Speech Communication* **55** (2013) 667–690. 1203
- 1204 1204
- 1205 [38] P. Birkholz: A survey of self-oscillating lumped-element models of the vocal folds. In: B. J. Kröger, P. Birkholz, eds., *Studenttexte zur Sprachkommunikation: Elektronische Sprachsignalverarbeitung*, 2011, 47–58. 1205
- 1206 1206
- 1207 [39] M. Zaňartu, L. Mongeau, G. R. Wodicka: Influence of acoustic loading on an effective single mass model of the vocal folds. *The Journal of the Acoustical Society of America* **121** (2007) 1119–1129. 1207
- 1208 1208
- 1209 [40] J. van den Berg, J. T. Zantema, P. Doornenbal: On the air resistance and the Bernoulli effect of the human larynx. *Journal of the Acoustical Society of America* **29** (1957) 626–631. 1209
- 1210 1210
- 1211 [41] L. P. Fulcher, R. C. Scherer, T. Powell: Pressure distributions in a static physical model of the uniform glottis: Entrance and exit coefficients. *The Journal of the Acoustical Society of America* **129** (2011) 1548–1553. 1211
- 1212 1212
- 1213 [42] T. Lukkari, J. Malinen: Webster’s equation with curvature and dissipation. ArXiv e-prints, arXiv:1204.4075, 2013. 1213
- 1214 1214
- 1215 [43] A. Aalto, T. Lukkari, J. Malinen: Acoustic wave guides as infinite-dimensional dynamical systems. *ESAIM: Control, Optimisation and Calculus of Variations* **21** (2015) 324–347. 1215
- 1216 1216
- 1217 [44] T. Lukkari, J. Malinen: A posteriori error estimates for Webster’s equation in wave propagation. *Journal of Mathematical Analysis and Applications* **427** (2015) 941–961. 1217
- 1218 1218
- 1219 [45] T. Hélie, X. Rodet: Radiation of a pulsating portion of a sphere: application to horn radiation. *Acta Acustica united with Acustica* **89** (2003) 565–577. 1219
- 1220 1220
- 1221 [46] P. Birkholz, D. Jackel, B. Kröger: Simulation of losses due to turbulence in the time-varying vocal system. *IEEE Transactions on Audio, Speech, and Language Processing* **15** (2007) 1218–1226. 1221
- 1222 1222
- 1223 [47] D. Aalto, O. Aaltonen, R.-P. Happonen, P. Jääsaari, A. Kivelä, J. Kuortti, J.-M. Luukinen, J. Malinen, T. Murtola, R. Parkkola, J. Saunavaara, T. Soukka, M. Vainio: Large scale data acquisition of simultaneous MRI and speech. *Applied Acoustics* **83** (2014) 64–75. 1223
- 1224 1224
- 1225 1225
- 1226 1226
- 1227 1227
- 1228 1228
- 1229 1229
- 1230 1230
- 1231 1231
- 1232 1232
- 1233 1233
- 1234 1234
- 1235 1235
- 1236 1236
- 1237 1237
- 1238 1238
- 1239 1239

- 1199 [48] B. Story, I. Titze, E. Hoffman: Vocal tract area func- 1258
1200 tions from magnetic resonance imaging. *The Journal* 1259
1201 *of the Acoustical Society of America* **100** (1996) 537– 1260
1202 554.
- 1203 [49] B. H. Story, I. R. Titze, E. A. Hoffman: Vocal tract 1261
1204 area functions for an adult female speaker based on 1262
1205 volumetric imaging. *The Journal of the Acoustical* 1263
1206 *Society of America* **104** (1998) 471–487. 1264
- 1207 [50] B. H. Story, I. R. Titze: Parameterization of vocal 1265
1208 tract area functions by empirical orthogonal modes. 1266
1209 *Journal of Phonetics* **26** (1998) 223–260. 1267
- 1210 [51] A. Kivelä: Acoustics of the Vocal Tract: MR image 1268
1211 segmentation for modelling. Master’s thesis, Aalto 1269
1212 University School of Science, Espoo, Finland, 2015.
- 1213 [52] A. Ojalampi, J. Malinen: Automated segmentation 1270
1214 of upper airways from MRI: Vocal tract geometry 1271
1215 extraction. *Proceedings of BIOIMAGING 2017*, 2017, 1272
1216 77–84. 1273
- 1217 [53] P. M. Morse, K. U. Ingard: *Theoretical acoustics*. 1274
1218 McGraw-Hill, 1968. 1275
- 1219 [54] B. Cranen, L. Boves: Pressure measurements dur- 1276
1220 ing speech production using semiconductor miniature 1277
1221 pressure transducers: Impact on models for speech 1278
1222 production. *The Journal of the Acoustical Society of* 1279
1223 *America* **77** (1985) 1543–1551. 1280
- 1224 [55] B. Cranen, L. Boves: On subglottal formant analysis. 1281
1225 *The Journal of the Acoustical Society of America* **81** 1282
1226 (1987) 734–746.
- 1227 [56] I. R. Titze: Physiologic and acoustic differences be- 1283
1228 tween male and female voices. *The Journal of the* 1284
1229 *Acoustical Society of America* **85** (1989) 1699–1707. 1285
- 1230 [57] D. Scimarella, C. d’Alessandro: On the acoustic sen- 1286
1231 sitivity of a symmetric two-mass model of the vo- 1287
1232 cal folds to the variation of control parameters. *Acta* 1288
1233 *Acustica united with Acustica* **90** (2004) 746–761. 1289
- 1234 [58] P. Lieberman, R. Knudson, J. Mead: Determination 1290
1235 of the rate of change of fundamental frequency with 1291
1236 respect to subglottal air pressure during sustained 1292
1237 phonation. *The Journal of the Acoustical Society of* 1293
1238 *America* **45** (1969) 1537–1543. 1294
- 1239 [59] I. R. Titze: On the relation between subglottal pres- 1295
1240 sure and fundamental frequency in phonation. *The* 1296
1241 *Journal of the Acoustical Society of America* **85** 1297
1242 (1989) 901–906. 1298
- 1243 [60] P. Alku: Glottal inverse filtering analysis of human 1299
1244 voice production - a review of estimation and param- 1300
1245 eterization methods of the glottal excitation and their 1301
1246 applications. *Sadhana* **36** (2011) 623–650. 1302
- 1247 [61] V. Havu, J. Malinen: The Cayley transform as a time 1303
1248 discretization scheme. *Numerical Functional Analysis* 1304
1249 *and Optimization* **28** (2007) 825–851. 1305
- 1250 [62] I. R. Titze: Regulating glottal airflow in phonation: 1306
1251 Application of the maximum power transfer theorem 1307
1252 to a low dimensional phonation model. *The Journal* 1308
1253 *of the Acoustical Society of America* **111** (2002) 367– 1309
1254 376.
- 1255 [63] I. R. Titze: Parameterization of the glottal area, glot- 1310
1256 tal flow, and vocal fold contact area. *The Journal of* 1311
1257 *the Acoustical Society of America* **75** (1984) 570–580.
- [64] P. Alku: Glottal wave analysis with pitch syn- 1258
chronous iterative adaptive inverse filtering. *Speech* 1259
Communication **11** (1992) 109–118. 1260
- [65] H. Pulakka: Analysis of human voice production us- 1261
ing inverse filtering, high-speed imaging, and elec- 1262
troglottography. Master’s thesis, Helsinki University 1263
of Technology, Espoo, Finland, 2005. 1264
- [66] A. Aalto, P. Alku, J. Malinen: A LF-pulse from 1265
a simple glottal flow model. *Proceedings of the* 1266
6th International Workshop on Models and Analy- 1267
sis of Vocal Emissions for Biomedical Applications 1268
(MAVEBA2009), Florence, 2009, 199–202. 1269
- [67] M. Berouti, D. Childers, A. Paige: Glottal area ver- 1270
sus glottal volume-velocity. *IEEE International Con-* 1271
ference on Acoustics, Speech, and Signal Processing 1272
ICASSP ’77 (1977) **2** 33–36. 1273
- [68] S. Granqvist, S. Hertegård, H. Larsson, J. Sund- 1274
berg: Simultaneous analysis of vocal fold vibration 1275
and transglottal airflow: exploring a new experimen- 1276
tal setup. *Journal of Voice* **17** (2003) 319–330. 1277
- [69] N. Ruty, X. Pelorson, A. van Hirtum: Influence of 1278
acoustic waveguides lengths on self-sustained oscilla- 1279
tions: Theoretical prediction and experimental vali- 1280
dation. *Proceedings of Acoustics ’08*, Paris, June 29- 1281
July 4, 2008, 1243–1247. 1282
- [70] S. M. Lulich, H. Arsikere: Tracheo-bronchial soft tis- 1283
sue and cartilage resonances in the subglottal acoustic 1284
input impedance. *Journal of the Acoustical Society of* 1285
America **137** (2015) 3436–3446. 1286
- [71] B. D. Erath, S. D. Peterson, M. Zaňartu, G. R. Wod- 1287
icka, M. W. Plesniak: A theoretical model of the pres- 1288
sure field arising from asymmetric intraglottal flows 1289
applied to a two-mass model of the vocal folds. *The* 1290
Journal of the Acoustical Society of America **130** 1291
(2011) 389–403. 1292
- [72] P. Punčochářová-Pořízková, K. Kozel, J. Horáček, 1293
J. Fürst: Numerical simulation of unsteady compres- 1294
sible low Mach number flow in a channel. *Engi-* 1295
neering Mechanics **17** (2010) 83–97. 1296
- [73] P. Šidlof, J. Horáček, V. Řidký: Parallel CFD simu- 1297
lation of flow in a 3D model of vibrating human vocal 1298
folds. *Computers & Fluids* **80** (2013) 290–300. 1299
- [74] T. Vampola, J. Horáček, A.-M. Laukkanen, J. G. 1300
Švec: Human vocal tract resonances and the 1301
corresponding mode shapes investigated by three- 1302
dimensional finite-element modelling based on CT 1303
measurement. *Logopedics Phoniatrics Vocology* **40** 1304
(2013) 1–10. 1305
- [75] T. Vampola, A.-M. Laukkanen, J. Horáček, J. G. 1306
Švec: Finite element modelling of vocal tract changes 1307
after voice therapy. *Applied and Computational Me-* 1308
chanics **5** (2011) 77–88. 1309